Accepted Manuscript

Blue light emitting Y2O3:Tm3+ nanophosphors with tunable morphology obtained by bio-surfactant assisted sonochemical route

K.N. Venkatachalaiah, H. Nagabhushana, G.P. Darshan, R.B. Basavaraj, B. Daruka Prasad, S.C. Sharma

PII: S1386-1425(17)30302-5
DOI: doi: 10.1016/j.saa.2017.04.033
Reference: SAA 15086

To appear in: *Spectrochimica Acta Part A: Molecular and Biomolecular Spectroscopy*

Received date: 13 September 2016
Revised date: 8 April 2017
Accepted date: 18 April 2017

Please cite this article as: K.N. Venkatachalaiah, H. Nagabhushana, G.P. Darshan, R.B. Basavaraj, B. Daruka Prasad, S.C. Sharma , Blue light emitting Y2O3:Tm3+ nanophosphors with tunable morphology obtained by bio-surfactant assisted sonochemical route. The address for the corresponding author was captured as affiliation for all authors. Please check if appropriate. Saa(2017), doi: 10.1016/j.saa.2017.04.033

This is a PDF file of an unedited manuscript that has been accepted for publication. As a service to our customers we are providing this early version of the manuscript. The manuscript will undergo copyediting, typesetting, and review of the resulting proof before it is published in its final form. Please note that during the production process errors may be discovered which could affect the content, and all legal disclaimers that apply to the journal pertain.

ACCEPTED MANUSCRIPT

Blue light emitting $Y_2O_3:Tm^{3+}$ nanophosphors with tunable morphology obtained by bio-surfactant assisted sonochemical route

K. N. Venkatachalaiah[1, 2], H. Nagabhushana[3], G.P. Darshan[4], R.B. Basavaraj[3], B. Daruka Prasad[5], S.C. Sharma[6,7]

[1]Department of Physics, Amrita School of Engineering, Amrita Vishwavidyapeetham, Amrita university, Bengaluru- 560035, India
[2]Research and Development Center, Bharathiar University, Coimbatore 641046, India
[3]Prof. C.N.R. Rao Centre for Advanced Material Science, Tumakuru University, Tumakuru-572103, India
[4]Department of Physics, Acharya Institute of Graduate Studies, Bangalore 560 107, India
[5]Department of Physics, B.M.S. Institute of Technology and Management, VTU affiliated, Bengaluru-560 064, India
[6]Department of Mechanical Engineering Jain University, Advisor, Jain group of Institutions, Bangalore - 560069, India
[7]Advisor, Avinashilingam University for Women, Coimbatore -641043, Tamilnadu, India.

Abstract

Modified sonochemical route was used to prepare $Y_2O_3:Tm^{3+}$ (1-11 mol %) nanophosphor using *Mimosa pudica* (*M.P.*) leaves extract as bio-surfactant. The prepared samples were exhibited high crystalline nature with various morphologies. This was due to sonochemical experimental reaction took place between cavitation bubbles and nearby solution. The average crystallite sizes of the prepared samples were about 15 nm to 21 nm as obtained from PXRD and TEM analysis. The ultraviolet visible absorption spectra showed prominent bands with an energy gap varied from 5.73 eV to 5.84 eV. Photoluminescence (PL) emission spectra shows the prominent blue light emission peak at ~ 456 nm attributed to $^1D_2 \rightarrow {}^3F_4$ transitions of Tm^{3+} ions. The Judd–Ofelt intensity parameters were estimated by using PL emission spectra. The photometric characteristics of the prepared compounds were very close to the blue colour of NTSC standards. So the results were fruitful in making use of $Y_2O_3:Tm^{3+}$ nanophosphor as an alternative material for effective blue component in WLED's.

Keywords: Sonochemical method; Mimosa pudica; Photoluminescence; Judd – Ofelt analysis.

*Corresponding Author: E-mail address: bhushanvlc@gmail.com (Dr. H. Nagabhushana)

ACCEPTED MANUSCRIPT

1. Introduction

In the recent years, synthesis of nanophosphors with low cost and high efficiency creates a new avenue for research community to develop components for efficient white light emitting diodes (LEDs) [1, 2]. Among them rare earth (RE) ions doped inorganic nanophosphors were explored as novel functional materials for display devices, catalysts, magnets, forensic and anti-counterfeiting applications due to their excellent optical, chemical and physical properties [3-5].

In addition, the well-defined architectural tuning of inorganic nanophosphors still a research focus due to the close interrelation between the chemical and physical properties of materials and their geometrical factors such as shape, dimensionality, size and surface. Regular patterned morphologies not only control their properties but also enhance the efficiency for the most of the applications due to increased surface area to volume ratio and quantum confinement effects [6]. Therefore, there were several wet chemical methods viz., combustion, sol–gel, co-precipitation, and hydrothermal methods were employed but still faces issue of controlled morphologies, uniform size and compositions [7-11]. Hence selection of appropriate synthesis method to fabricate nanostructured materials with various morphologies creates numerous interests for scientific community. Much research is necessary for the development of novel and versatile synthesis routes which are readily adaptable for the synthesis of several nanostructured materials with the possibility to extend for the industry needs. Among the various methods, ultrasound assisted sonochemical route was powerful for the synthesis of nanostructured materials. To initiate chemical reactions ultrasound irradiation provides moderately remarkable reaction conditions including short duration of time, high temperature and pressure to end up with a desired nanostructured products. The high intensity ultrasound force to acoustic cavitation including formation, growth and implosive collapse of bubbles in reaction mixture leads to various morphologies [12].

ACCEPTED MANUSCRIPT

Yttrium oxide (Y_2O_3) was considered to be one of the best hosts due its wide spread applications in the field of flat panels, optoelectronic devices, photo electronic industry and biotechnological applications [13–16]. The RE ions doped Y_2O_3 materials shows exceptional luminescence properties such as narrow emission lines, long luminescence efficiency and high color purity with high chemical and thermal stability [17, 18]. Among the various RE ions, Tm^{3+} ions were considered to be the best dopants because of their excellent spectroscopic benefits and donor as well as acceptor nature in cross- relaxation energy transfer mechanism which leads to the avoid of unnecessary relaxation channels. Therefore, the selection of Tm^{3+} ions as dopants creates interest due to its well known blue emission and simple transition states [19, 20].

The concept of green chemistry opens up as a new approach for the preparation of safer nanostructured materials. In this point of view, *memosa pudica* (*M.P.*) leaves extract was considered as a bio-surfactant for the preparation of Y_2O_3:Tm^{3+} (1-11 mol %) nanophosphor. *M.P.* belongs to the family of *Mimosae* which was scattered throughout India and mostly observed in moist surroundings and used in diagnosing astringent, acrid, cooling vulnerary, alexipharmic, diuretic antispasmodic diseases etc. [21 - 23]. The leaves were rich in phytochemicals such as tannins, steroids, saponins and flavonoids etc.

The present work is focused on the synthesis of doped Y_2O_3:Tm^{3+} (1-11 mol %) nanophosphor by facile ultrasound assisted sonochemical route using *M.P.* leaves extract as bio-surfactant. The effectiveness and unique properties of ultrasound for the fabrication of nanostructured materials was successfully explored. Also a detailed study was carried out to investigate the formation of unusual surface morphology of the product occurred due to various reaction conditions. Further to evaluate the potential applications of the prepared samples, the

ACCEPTED MANUSCRIPT

photometric properties (PL, CIE and CCT) of Y_2O_3:Tm^{3+} (1-11 mol %) nanophosphor were studied in detail.

2. Synthesis and characterization

Precursors used in the present study were Yttrium nitrate [(Y $(NO_3)_3$, Sigma Aldrich; 99.9%)], Thulium nitrate [($Tm(NO_3)_3$, Sigma Aldrich; 99.9%)] and NaOH procured from Sigma Aldrich. *M.P.* leaves extract was used as a surfactant. Fresh leaves of *M.P.* were collected and splashed many times with deionized water. The leaves were then dried in air and kept for 15-20 days at room temperature (RT). The dried leaves were crushed using agate mortar to get soft powder. The sample was then introduced to successive solvent removal using thimble and Soxhlet apparatus. Further, it was refluxed several times with the double distilled water for 72 h. Again with the help of rotary flash evaporator the obtained extract was filtered. The deionized water and the unwanted products were thrashed away on water bath and lastly it was dried in a dessicator for further use as a fuel. The extract of *M.P.* (1 g) was dissolved uniformly in 90 ml of deionized water by using magnetic stirrer. The precursor solution of yttrium nitrate and thulium nitrate were taken in cylindrical beaker and mixed homogeneously using magnetic stirrer for ~ 15 min. Further, different concentration of *M.P.* extract (5- 30 % W/V) was added to the resultant mixture slowly and pH level (1, 5, 7, and 9) of the solution was maintained by adding NaOH under constant stirring. The obtained solution was irradiated with high intensity (300 W/cm^2) ultrasonic radiation operating at ultrasonic frequency of ~ 20 kHz and irradiation time of 1 - 6 h at a fixed temperature of 80 ^oC. After sonication, the precipitate was filtered using double distilled water and alcohol. The obtained powder was dried at 80 ^oC for 3 h in a hot air oven and further heat treated at ~ 700 ^oC for 3 h. Fig.1. shows the schematic diagram for the synthesis of Tm^{3+} doped Y_2O_3 nanophosphor.

ACCEPTED MANUSCRIPT

PXRD measurements were carried out on a Shimadzu made (XRD - 7000) Powder X–ray diffractometer in the 2θ range of 20-70° using Cu-Kα (λ = 1.54178 Å) radiation. The electron microscopy images were recorded by using Hitachi (TM - 3000 and H - 8100). Perkin Elmer (SL 159) UV–Vis spectrophotometer was utilized to UV – visible data. The PL excitation and emission spectra of the prepared samples were recorded by using Fluorolog-3 Jobin Yvon Spectroflourimeter with 450 W Xenon lamp as an excitation source in the range 500 – 750 nm.

3. Results and discussion

Fig. 2. shows the SEM micrographs of Y_2O_3:Tm^{3+} (3 mol %) nanophosphor synthesized with different sonication time (1 – 6 h) while concentration *M.P.* surfactant and pH value of the solution were fixed at 30 % W/V and 9 respectively. When ultrasound irradiation time was at 1h and 2 h, spike - like structures were observed (Fig.2 (a & b)). As the irradiation was extended to 3 h and 4 h, spike - like structures were undergo growth and start oriented in order direction was observed in Fig.2 (c & d). Further, when the ultrasonic irradiation time was still prolonged to 5 – 6 h, the spike - like structures were orderly oriented in all direction and resembles to surface of jackfruit was shown in Fig.2 (e & f). Thus it was confirmed from the aforementioned results that the ultrasound irradiation time significantly affect the morphology of the product. In an ultrasound assisted sonochemical synthesis route involves two types reactions (i) reaction between cavitation bubble and nearby solution which leads to high crystalline product and (ii) reaction take place within the collapsing bubbles leads to amorphous material. In the present work, the synthesized samples were highly crystalline nature with various morphologies evidences the reaction takes place in interfacial region involved in the formation of the Y_2O_3:Tm^{3+} (3 mol %) nanophosphor.

ACCEPTED MANUSCRIPT

Fig.3. shows the effect of various concentration of *M.P.* extract on morphology of the prepared Y_2O_3:Tm^{3+} (3 mol %) nanophosphor with 6 h of ultrasonic irradiation time and pH = 9. When the *M.P.* extract concentration is 5 and 10 % W/V, spherical shaped structures to form "hollow ball" like structure was observed (Fig. 3 (a & b)). When the concentration of *M.P.* extract was increased to 15 – 20 % W/V, spherical shaped surface structures undergo growth to form spike like structures were shown in Fig. 3 (c & d)). Further, increase of *M.P.* concentration to 30 % W/V, spikes were orderly oriented to form "nano-Koosh ball" like structure was observed (Fig.3 (e)). Schematic representation of formation of Y_2O_3:Tm^{3+} "nano-Koosh ball" like structure with different concentration of *M.P.* was shown in Fig.4. The effect of *M.P.* extract on formation of structures was explained based on the egg box model, where the polymeric network of the contents of the *M.P.* wrap into complex network of in which the Y_2O_3:Tm^{3+} ions gets trapped leaving behind the various structures as shown in Fig. 5.

The pH value of the solution was varied by adding NaOH to the reaction mixture and it could greatly affect on morphology of the prepared product by altering size and shape due to various factors including crystal- face attraction, electrostatic and dipolar fields associated with the aggregate, Vander Waals forces, intrinsic structures and external factors leads to hierarchical structures. It is noteworthy that, the pH of the precursor solution was maintained at 1 and 3, there was a formation of fiber-like structures was observed (Fig.6). As the pH of the solution was increased to 5, mix of fiber and spike - like structures were observed. Further, pH was increased to 7 and 9, these fibers - like structures were dominated by further growth and were oriented in different directions were observed in Fig. 6. These results were evident that the pH value has played vital role in tuning the morphology of the product. The schematic representation for

ACCEPTED MANUSCRIPT

demonstrate the nucleation, growth and collapse of a stimulated by ultrasound irradiation was shown in Fig.7.

To know the effect of ultrasound irradiation, mechanical stirring for different time period (1 – 6 h) was applied during the preparation of Y_2O_3:Tm^{3+} nanophosphor. The irregular flakes with small agglomerates (irregular) with micrometer sized particles were observed (Fig.8). It evidence that, the ultrasound irradiation leads to stabilized cavitation for the formation of well-crystallized structures. Hence, ultrasound irradiation assisted sonochemical route was a synergistic approach to synthesize self assembled Y_2O_3: Tm^{3+} structures with tunable size.

To evaluate the crystallite size, interplanar distance and crystallinity of the product, analysis of TEM, HRTEM and SAED patterns of Y_2O_3:Tm^{3+} (3 mol %) nanophosphor was studied (Fig.9 (a-e)). The TEM images evident that the formation of agglomerated cubic- flake like structures (Fig.9 (a) and (b)). The HRTEM images of Y_2O_3:Tm^{3+} (3 mol %) nanophosphor was shown in Fig.9 ((c) and (d)). The estimated crystallite size was found to be ~ 0.28 nm corresponds to (222) plane. The obtained SAED pattern (Fig.9 (e)) shows the high crystallinity of the prepared sample and the spots were well indexed to (211), (222), (400), (411), (420), (332), (440), (611) and (622) planes.

The PXRD profiles of Y_2O_3:Tm^{3+} (1-11 mol %) nanophosphor were shown in Fig. 10 (a). The sharp and intense diffraction profiles were confirm the formation of single cubic phase of Y_2O_3 and were well matched with standard JCPDS card No. 88-1040 [24]. With increase of dopant Tm^{3+} concentrations, line broadening and peak shifting (222) towards higher angle side was observed (Fig. 10 (b)). No impurity peaks were observed, indicating that dopant Tm^{3+} ions were homogeneously mixed and occupied vacancy site of the host Y_2O_3 matrix. The line

ACCEPTED MANUSCRIPT

broadening of diffracted peaks were used to estimate the crystallite size of the prepared samples by using Debye – Scherrer's relation [25]:

$$D = K\lambda / \beta \cos\theta \qquad \text{---------- (1)}$$

Where 'K' is the shape parameter, for perfect spherical particles the value of K is 1 otherwise it is taken as 0.87 to 0.9 for the particles of deviated from spherical shape. In our case K is taken as 0.89. λ ; the wavelength of the X-rays, β ; the full- width at half maximum (FWHM) and θ ; the angle of diffraction. The average crystallite size of Y_2O_3:Tm^{3+} (1-11 mol %) nanophosphor were estimated and listed in Table 1. The line broadening of PXRD peaks were mainly due to micro-strain present in the samples. Williamson – Hall (W - H) fitting method was used to estimate the crystallite size and micro – strain present in the prepared samples using following relation [26]:

$$\beta \cos\theta = \varepsilon\left(4 \sin\theta\right) + \frac{\lambda}{D} \qquad \text{---------- (2)}$$

where 'β' (FWHM in radians) was measured for different PXRD lines corresponding to different planes, ε ; the strain developed, D; the crystallite size and θ; Bragg's diffraction angle. The average crystallite size and micro – strain present in the samples were estimated and tabulated in Table 1. The W-H plots were shown in Fig. 10 (c).

The cubic structure of the prepared samples was confirmed through structural Rietveld refinement by using *Fullprof Program*. The results were good agreement with observed and calculated PXRD patterns (Fig.10 (d)). The structural refinement quality was measured by a parameter called goodness of fit (GoF). In the present work, estimated GoF was found to be ~ 0.73. The estimated structural parameters of the prepared samples were estimated and given in

ACCEPTED MANUSCRIPT

Table.2. The schematic diagram of unit cell of prepared Y_2O_3 nanophosphor was shown in inset Fig.10 (e). The Visualization for Electronic and Structural Analysis (VESTA) program was used to model unit cell [27]. The prepared Y_2O_3 nanophosphor has a cubic phase with a space group Ia – 3 and point – group symmetry m-3. The unit cell 16 units and 32 cations. The cubic structure contains two symmetry cations sites C_2 and C_{3i}, both co-ordinates with six – fold with oxygen, as shown in Fig.2 (d). The C_2 and C_{3i} sites were arranged over two Wyckoff positions 8b and 24d local symmetry respectively. Wyckoff 48e positions were occupied by Oxygen ions. To understand effective substitution of dopant Tm^{3+} ions at Y^{3+} symmetry site, the acceptable percentage difference was estimated by using following relation [25]:

$$D_r = \frac{R_m - R_d}{R_m} \qquad \text{---------- (3)}$$

where R_m and R_d; radii of host material and dopant ion respectively. The ionic radii of Tm^{3+} and Y^{3+} ions were close to each other and estimated value of D_r was found to be ~ 2.13 %. This shows that dopant Tm^{3+} ions were substituted easily at Y^{3+} symmetry site.

The diffuse reflectance (DR) spectra of pure and Y_2O_3: Tm^{3+} (1-11 mol %) nanophosphor were recorded against standard $BaSO_4$ as a reference sample (Fig. 11). The spectra exhibits a broad absorption band at ~ 223 nm ($^3H_6 \rightarrow {}^1H_6$) was observed for both pure and doped samples which confirm that light having absorbed in this particular wavelength. Further, the other bands observed at ~ 328 nm ($^3H_6 \rightarrow {}^1D_2$), 528 nm ($^3H_6 \rightarrow {}^1G_4$) and 727 nm ($^3H_6 \rightarrow {}^3F_3$) in the DR spectra were due to meta-stable energy states formed in between valence and conduction bands by the Tm^{3+} ions. However, in case of doped samples, the absorption band shifts toward lower wavelength side (blue shift) due crystallite size effect [28].

ACCEPTED MANUSCRIPT

From DR spectra, the direct energy band gap (E_g) was estimated by using Kubelka–Munk theory [29]. The ratio of the light scattered from a thick layer of powder material and an ideal non-absorbing reference sample was recorded with respect to the wavelength λ [29]:

$$R_\infty = R_{sample} / R_{reference} \quad \text{---------- (4)}$$

The Kubelka–Munk function F(R∞) relay the diffuse reflectance of the sample (R_∞), absorption coefficient (K) and scattering coefficient (S) and was specified by the relation:

$$F(R_\infty) = \frac{(1-R_\infty)^2}{2R_\infty} = \frac{K}{S} \quad \text{---------- (5)}$$

The E_g and linear absorption coefficient α of a sample was associated through the well-known Wood - Tauc relation [30]:

$$\alpha h\nu = C_1 (h\nu - E_g)^{1/2} \quad \text{---------- (6)}$$

where hν ; the photon energy and C_1 ; proportionality constant. When the powder sample scatters in completely diffuse behavior (or when it is illuminated at 60° incidence), the absorption coefficient (K) becomes equal to 2α. Considering the scattering co - efficient (S) as constant with respect to wavelength, and using Eqs. (5) and (6), the following relation can be expressed:

$$[F(R_\infty) h\nu]^2 = C_2 (h\nu - E_g) \quad \text{---------- (7)}$$

From the plot of $[F(R_\infty)\, h\nu]^2$ versus hν as shown in the Fig. 11(b), the value of E_g was obtained by extrapolating the linear fitted regions to $[F(R_\infty)\, h\nu]^2 = 0$. The estimated E_g values from the DR spectra using K–M function $F(R_\infty)$ were tabulated in Table 1. From the obtained E_g values, it was evident that the band gap values were tuned after increasing the dopant concentration.

Fig.12 (a) shows the PL excitation spectra of Y_2O_3: Tm^{3+} (1 - 11 mol %) nanophosphor under emission wavelength at 456 nm. The spectra exhibits peaks at 359 and 300 nm were attributed to $^3H_6 \rightarrow {}^1D_2$ and $^3H_6 \rightarrow {}^1I_6$ transitions of Tm^{3+} ions respectively. Fig.12 (b) shows the

ACCEPTED MANUSCRIPT

PL emission spectra of Y_2O_3: Tm^{3+} (1-11 mol %) nanophosphor under the excitation wavelength of 359 nm at RT. The spectra exhibit intense peak at ~ 456 nm (blue-light region) and a weak peak at ~ 488 nm corresponding to the $^1D_2 \rightarrow {}^3F_4$ and $^1G_4 \rightarrow {}^3H_6$ transition of Tm^{3+} ions respectively [19]. It was observed that, PL emission intensity of Y_2O_3: Tm^{3+} nanophosphor at 456 nm increases upto 3 mol % and afterwards diminishes due to phenomena called concentration quenching effect (Inset Fig.13). Concentration quenching phenomenon was due to transfer of energy from one activator to the nearby ions. The distance between the two Tm^{3+} ions in Y_2O_3 host was estimated by using critical energy transfer distance relation [31]:

$$R_c = 2\left(3V/4\pi N X_c\right)^{1/3} \quad \text{---------- (8)}$$

where V; unit cell volume, X_c; critical concentration of Tm^{3+} ions and N; number of crystallographic sites per unit cell. In the present case, calculated value of R_c was found to be ~ 8.975 Å. The calculated value of R_c was greater than 5Å indicates that electric multipolar interaction is responsible for concentration quenching. The electric multipolar interaction was estimated by using the following relation [32]:

$$\frac{I}{\chi} = K\left[1+\beta(\chi)^{\frac{Q}{3}}\right]^{-1} \quad \text{---------- (9)}$$

where χ ; concentration of Tm^{3+} ions, Q ; a constant for electric multipolar interaction and K & β ; constants for the given host crystal under the same excitation condition. The value of *Q* was estimated by plotting log (I/x) v/s log (x) and was shown in Fig.13. The figure clearly confirms that the relation was approximately linear and the value of slope was about -0.717. The calculated value Q was found to be 2.151 by linear fitting using Eq. (9) and was less than 6, . This finding indicates that dipole–quadrupole interaction was main reason for the concentration quenching in Y_2O_3:Tm^{3+} (1-11 mol %) nanophosphor.

ACCEPTED MANUSCRIPT

The Judd–Ofelt (J - O) analysis from PL emission spectra was an effective tool for evaluating the RE ions concentration dependence spectroscopic parameters of various hosts [33, 34]. J - O intensity parameters (Ω_2 and Ω_4) were explored to know the bonding character of RE ions with its surrounding ligands and site symmetry of dopant [35]. The integrated radiative emission rates between two transitions $^1D_2 \rightarrow {}^3F_4$ and $^1G_4 \rightarrow {}^3H_6$ was given by following relation [36].

$$\frac{A_{0\text{-}2,4}}{A_{0\text{-}1}} = \left[\frac{I_{0\text{-}2,4}}{I_{0\text{-}1}}\right]\left[\frac{h\nu_{0\text{-}1}}{h\nu_{0\text{–}2,4}}\right] \qquad \text{--------- (10)}$$

where $I_{0\text{–}2,4}$; the integrated emission intensity and $h\nu_{0\text{-}J}$; the energy corresponding to transition $^1D_2 \rightarrow {}^3F_4$ and $^1G_4 \rightarrow {}^3H_6$. The forced electric dipole transition as a function of J - O intensity parameters was expressed as:

$$A_{0\text{-}2,4} = \frac{64\pi^4\left(\nu_{0\text{-}2,4}\right)^3 e^2}{3hc^3}\left(\frac{1}{4\pi\varepsilon_0}\right)\chi \sum_{J=2,4}\Omega_J \left\langle {}^1D_0 \left| U^{(J)} \right| {}^3F_4 \right\rangle^2 \qquad \text{----- (11)}$$

where $\chi = n(n^2+2)^2/9$; the Lorentz local field correction factor and n ; the refractive index of host lattice. $\left\langle {}^1D_0 \left| U^{(J)} \right| {}^3F_4 \right\rangle^2$; the square matrix elements corresponding transition of dopant Tm^{3+} ions [19]. Thus, by equating Eq. (10) and Eq. (11), intensity parameters (Ω_2 and Ω_4) of Y_2O_3:Tm^{3+} (1- 11 mol %) nanophosphor were evaluated and given in Table 3. The estimated J - O intensity parameters Ω_2 and Ω_4 were due to short and long-range effect respectively. The value of Ω_2 predicts the maximum covalence among the Tm^{3+} ions and the neighboring O^{2-}. The results obtained from J–O intensity parameters ($\Omega_2 > \Omega_4$) indicates the existence of covalence between the Tm^{3+} ion and the ligands along with surrounding the metal ion sites. Further, J - O intensity parameters (Ω_2 and Ω_4) of Y_2O_3:Tm^{3+} (1- 11 mol %) nanophosphor were utilized to estimate the radiative parameters such as transition probabilities (A_T), radiative life time (τ_R) and branching

ACCEPTED MANUSCRIPT

ratio ($\beta(\psi_J)$) according to literature [37]. The radiative transition probability (A_T) was determined by using the relation;

$$A_T(\psi_J) = \sum_{J'} A_{J-J'} \qquad \text{---------- (12)}$$

The radiative lifetime (τ_{rad}) of an excited state can be expressed as

$$\tau_{rad}(\psi_J) = \frac{1}{A_T(\psi_J)} \qquad \text{---------- (13)}$$

The branching ratio $\beta(\psi_J)$ corresponding to the emission from an excited level to its lower level was given by [37];

$$\beta(\psi_J) = \frac{A(\psi_J, \psi'_{J'})}{A_T(\psi_J)} \qquad \text{---------- (14)}$$

The measured branching ratio values for Tm^{3+} doped Y_2O_3 nanophosphor was found to be ~ 1 ≥ 0.50. The value suggests that present nanophosphor can emit laser radiation more effectively and suitable for blue emitting display devices.

To evaluate the color emission of the prepared product the Commission International de I'Eclairage (CIE) 1931 chromaticity co- ordinates were calculated and values were tabulated in inset of Fig.14 (a). CIE diagram of Y_2O_3:Tm^{3+} (1- 11 mol %) nanophosphor, it was clearly observed that chromaticity co-ordinates were positioned in the blue region and found to be close to the standard NTSC coordinates (Fig.14 (a)). Also to estimate the applicability of the obtained nanophosphor, correlated color temperature (CCT) was calculated by using CIE coordinates (Fig. 14(b)). The light emitted can be converted in terms of CCT by using the McCamy empirical formula [38]. If the lamp CCT value was less than 5000 K then it was considered as "warm" light sources and the lamps with CCT value greater than 5000 K was considered as "cool" in appearance [39]. The estimated CCT values were given in inset of Fig. 14 (b). The quantum

ACCEPTED MANUSCRIPT

efficiency (QE) of the optimized Y_2O_3:Tm^{3+} (3 mol %) nanophosphor was estimated by the method described by De Mello [40] and Palsson [41]:

$$QE = \frac{\text{Number of photons emitted}}{\text{Number of photons absorbed}} = \frac{E_c - E_a}{L_a - L_c} \quad \text{------- (15)}$$

where, E_C ; the integrated luminescence of the phosphor caused by direct excitation, E_a ; the integrated luminescence from the empty integrating sphere (blank, without sample), L_a; the integrated excitation profile from the empty integrating sphere, L_c; the integrated excitation profile when the sample is directly excited by the incident beam. The QE for the optimized Y_2O_3:Tm^{3+} (3 mol %) nanophosphor with 359 nm excitation was estimated by integrated emission counts from the 400-600 nm. The estimated value of QE was found to be ~ 47 %, suggest the high QE of the prepared sample. However, in our previous studies the QE was found to be 65 %, 61 % for MgO: Dy^{3+} [42], CeO_2:Eu^{3+} [43] and $YAlO_3$:Ho^{3+} [44] respectively. Thus the present nanophosphor can be used a cool blue component in lighting and display devices.

4. Conclusions

Blue light emitting Tm^{3+} doped Y_2O_3 nanophosphor were prepared by modified sonochemical method using *Mimosa Pudica* plant extract as a bio-surfactant. Influence of various reaction parameters such as sonication time, surfactant concentration and pH of the precursor solution on the morphology of the product were studied in detail. PXRD and structural refinement parameters confirm the cubic phase of prepared samples. The electric dipole–quadrupole interaction was main reason for the concentration quenching in Y_2O_3:Tm^{3+} (1-11 mol %) nanophosphor. The photometric characterizations of prepared samples were estimated and found to be fruitful for the design of efficient blue component of white phosphors for display and lighting applications.

ACCEPTED MANUSCRIPT

Acknowledgement

The author Dr. H Nagabhushana thanks to VGST, Karnataka for the sanction of this Project.

References

[1] H.S. Jang, D.Y. Jeon, Optics Lett. 32 (2007) 3444-3446.
[2] J. Huang, Q. Li, D. Chen, Mater. Sci. Eng. B 172 (2) (2010) 108.
[3] M. Venkataravanappa, H. Nagabhushana, B. Daruka Prasad, G.P. Darshan, R.B. Basavaraj, G.R. Vijayakumar, Ultrason. Sonochem. 34 (2017) 803-820.
[4] G.P. Darshan, H.B. Premkumar, H. Nagabhushana, S.C. Sharma, B. Daruka Prasad, S.C. Prashantha, R.B. Basavaraj, J. Alloys Compd. 686 (2016) 577-587.
[5] G.P. Darshan, H.B. Premkumar, H. Nagabhushana, S.C. Sharma, S.C. Prashantha, B. Daruka Prasad, J. Colloid Interface Sci. 464 (2016) 206.
[6] A. P. Alivisatos, Science, 271 (1996) 933–937.
[7] J. Hu, T. W. Odom, C. M. Lieber, Acc. Chem. Res. 32 (1999) 435–445.
[8] Y. Xia, Y. Xiong, B. Lim, S. E. Skrabalak, Angew. Chem.48 (2009) 60–103.
[9] S. Gai, C. Li, P. Yang, J. Lin, Chem. Rev.114 (2014) 2343–2389.
[10] C. Tana, B.Y. Liua, W. Lia, Y. Zhanga, Y. Hana, Mat. Sci. Eng. B, 176 (2011) 1251-1256.
[11] A. M. Kaczmarek, R. Van Deun, Chem. Soc. Rev. 42 (2013) 8835–8848.
[12] Jin Ho Bang, Kenneth S. Suslick, Adv. Mater. 22 (2010) 1039–1059
[13] S. Som, S.K. Sharma, S.P. Lochab, Mat. Res. Bull. 48 (2013) 844-851.
[14] S. Mukherjee, V. Sudarsan, P.U. Sastry, A. K. Patra, A. K. Tyagi, J. Lumin.145 (2014) 318-323.
[15] J.B. Prasanna Kumar, G. Ramgopal, Y.S. Vidya, K.S. Anantharaju, B. Daruka Prasad, S.C. Sharma, S.C. Prashantha, H.P. Nagaswarupa, D. Kavyashree, H. Nagabhushana, Spectrochim. Acta, Part A, 149 (2015) 687-697.
[16] J.B. Prasanna kumar, G. Ramgopal, Y.S. Vidya, K.S. Anantharaju, B. Daruka Prasad, S.C. Sharma, S.C. Prashantha, H.B. Premkumar, H. Nagabhushana, Spectrochim. Acta Part A, 141 (2015) 149–160.
[17] Xiaorong Zhang, Wenzhong Lu, Guifen Fan, Xiaohong Wang, Adv. Powd. Techn. 27 (2016) 295-298.
[18] Y. Li, Y. Chang, Y. F. Lin, Y. Lin, Appl. Phys. Lett. 89 (2006) 081110.
[19] G.P. Darshan, H.B. Premkumar, H. Nagabhushana, S.C. Sharma, S.C. Prashantha, H.P. Nagaswarupa, B. Daruka Prasad, Dyes Pigm. 131 (2016) 268-281.
[20] Xia Tian, Zhuang Weidong, Cui Xiangzhong, Zhao Chunlei, Teng Xiaoming, Huang Xiaowei, J. Rare Earths, 24 (2006) 141-144.
[21] R.B. Basavaraj, H. Nagabhushana, B. Daruka Prasad, S.C. Sharma, K.N. Venkatachalaiah, J. Alloys Compd. 690 (2017) 730-740.
[22] B. S. Chauhan , D. E. Johnson, Weed Bio. Mgt. 9 (2009) 38-45.
[23] C. Palacious, R.E. Reyes, Arch. Investig. Med. Mex. 22 (2) (1991) 163.

ACCEPTED MANUSCRIPT

ACCEPTED MANUSCRIPT

[24] Y. Liu, Y. Ruan, L. Song, W. Dong, C. Li, J. Alloys Compd. 581 (2013) 590-595.
[25] G.P. Darshan, H.B. Premkumar, H. Nagabhushana, S.C. Sharma, B. Daruka Prasad, S.C. Prashantha, Dyes and Pigments 134 (2016) 227-233.
[26] R.B. Basavaraj H. Nagabhushana B. Daruka Prasad, S.C. Sharma S.C. Prashantha B.M. Nagabhushana, Optik. 126 (2015) 1745-1756.
[27] S. Som, S. K. Sharma, J. Phys. D: Appl.Phys. 45 (2012) 415102-415113.
[28] S. Som, A. K. Kunti, Vinod Kumar, Vijay Kumar, S. Dutta, M. Chowdhury, S. K. Sharma, J. J. Terblans, H. C. Swart, J. .Appl.Phys. 115, (2014)193101-193114.
[29] A. E. Morales, E. S. Mora, U. Pal, Rev. Mex. Fis. S 53(5), (2007) 18.
[30] J. Tauc, A. Menth, J. Non-Cryst. Solids, 8 (1972) 569.
[31] B. Daruka Prasad, H. Nagabhushana, K. Thyagarajan, B.M. Nagabhushana, D.M. Jnaneshwara, S.C. Sharma, C. Shivakumara, N.O. Gopal, S.C. Ke, R.P.S. Chakradhar, J. Magn. Magn. Mater. 358-359 (2014) 132-141.
[32] M. Venkataravanappa, H. Nagabhushana, G.P. Darshan, B. Daruka Prasad, G.R. Vijayakumar, H.B. Premkumar, Udayabhanu, Ultrason. Sonochem. 33 (2016) 226-239.
[33] B. R. Judd, Phys. Rev. 127 (1962) 750.
[34] G. S. Ofelt, J. Chem. Phys. 37 (1962) 511.
[35] H.E. Heidepriem, D. Ehrt, J. Non-Cryst. Solids, 208 (1996) 205-216.
[36] H. J. Amith Yadav, B. Eraiah, H. Nagabhushana, G. P. Darshan, B. Daruka Prasad, S. C. Sharma, H. B. Premkumar, K. S. Anantharaju, G. R. Vijayakumar, ACS Sustainable Chem. Eng. DOI: 10.1021/acssuschemeng.6b01693.
[37] S. Dutta, S. Som, S. K. Sharma, RSC Adv. 5 (2015)7380- 7387.
[38] D.L. Monika, H. Nagabhushana, B.M. Nagabhushana, S.C. Sharma, K.S. Anantharaju, B. Daruka Prasad, C. Shivakumara, J. Alloys Compd. 648 (2015) 1051-1059.
[39] G. Ramakrishna, Ramachandra Naik, H. Nagabhushana, R.B. Basavaraj, S.C. Prashantha, S.C. Sharma, KS Anantharaju, Optik. 127 (2016) 2939-2945.
[40] J.C. De Mello, H.F. Wittmann, R.H. Friend, Adv. Mater. 9 (1997) 230–232.
[41] L.O. Palsson, A.P. Monkman, Adva. Mater. 14 (2002) 757–758.
[42] P.B. Devaraja, D.N. Avadhani, H. Nagabhushana, S.C. Prashantha, S.C. Sharma, B.M. Nagabhushana, H.P. Nagaswarupa, B.D. Prasad, Mat. Char. 97 (2014) 27-36.
[43] J. Malleshappa, H. Nagabhushana, S.C. Sharma, S.C. Prashantha, N. Dhananjaya, C. Shivakumara, B.M. Nagabhushana, J. Alloys Compd. 612 (2014) 425-434.
[44] H.B. Premkumar, B.S. Ravikumar, D.V. Sunitha, H. Nagabhushana, S.C. Sharma, M.B. Savitha, S. Mohandas Bhat, B.M. Nagabhushana, R.P.S. Chakradhar, Spectr. Acta Part A: Mol. Biomol. Spectr. 115 (2013) 234-243.

ACCEPTED MANUSCRIPT

Figure Captions:

Fig.1. Schematic representation for the preparation of Y_2O_3: Tm^{3+} (1 -11 mol %) nanophosphor using *M.P.* extract as a surfactant.

Fig. 2.SEM micrographs of Y_2O_3: Tm^{3+} (3 mol %) nanophosphor synthesized with different ultrasound irradiation time (1, 2, 3, 4, 5 and 6 h) while concentration *M.P.* surfactant and pH value of the solution were fixed at 30 % W/V and 9 respectively.

Fig.3. SEM micrographs of Y_2O_3: Tm^{3+} (3 mol %) nanophosphor synthesized with various concentration of *M.P.* surfactant (5, 10, 15, 20 and 30 % W/V) with 6 h of ultrasonic irradiation time and pH = 9.

Fig.4. Schematic representation for the formation of Y_2O_3: Tm^{3+} nanophosphor with different concentration of *M.P*.

Fig.5. Possible egg box model for the trapping of Y_2O_3:Tm^{3+} ions in the network of flavonoids.

Fig.6. SEM images of Y_2O_3: Tm^{3+} (3 mol %) nanophosphor with various pH values (1, 3, 5, 7 & 9) in the presence of *M.P.* (30 % W/V) and 6 h irradiation time.

Fig.7. The schematic representation to demonstrate nucleation, growth and collapse of bubbles by ultrasound irradiation.

Fig.8. SEM micrographs of Y_2O_3: Tm^{3+} (3 mol %) nanophosphor under mechanical stirring in the absence of *M.P.* surfactant with different time (a) 1 h, (b) 2 h, (c) 3 h, (d) 4 h, (e) 5 h & (f) 6 h.

Fig.9. (a & b) TEM images, (c & d) HRTEM images and (e) SAED pattern of Y_2O_3: Tm^{3+} (3 mol %) nanophosphor.

Fig.10. (a) PXRD patterns, (b) Shifting of (222) PXRD peak towards higher angle side, (c) W – H plots, (d) Rietveld refinement pattern (Inset: schematic representation of unit cell) and (e) cationic site symmetry of Y_2O_3:Tm^{3+} (1 – 11 mol %) nanophosphor.

Fig.11. (a) DR spectra and (b) Energy band gap (E_g) of Y_2O_3:Tm^{3+} (1- 11 mol %) nanophosphor.

Fig.12 (a). PL excitation spectra and emission of Y_2O_3:Tm^{3+} (1-11 mol %) nanophosphor.

Fig.13. Logarithmic plot of (I/X) as a function of the concentration (X) (Inset: Variation of PL intensity with Tm^{3+} concentration).

Fig.14 (a). CIE chromaticity diagram and (b) CCT diagram of Y_2O_3: Tm^{3+} (1-11mol %) nanophosphor (Inset: Their corresponding CIE and CCT co-ordinates).

ACCEPTED MANUSCRIPT

Table Captions:

Table.1. Estimated crystallite size, Full width half maxima (FWHM), strain and energy band gap (E_g) values of Y_2O_3: Tm^{3+} (1-11mol %) nanophosphor.

Table.2. Rietveld refinement data of Y_2O_3: Tm^{3+} (1-11 mol %) nanophosphor.

Table.3. Judd – Ofelt intensity parameters, radiative transition probability, radiative lifetime and branching ratio of Y_2O_3: Tm^{3+} (1-11 mol %) nanophosphor.

ACCEPTED MANUSCRIPT

ACCEPTED MANUSCRIPT

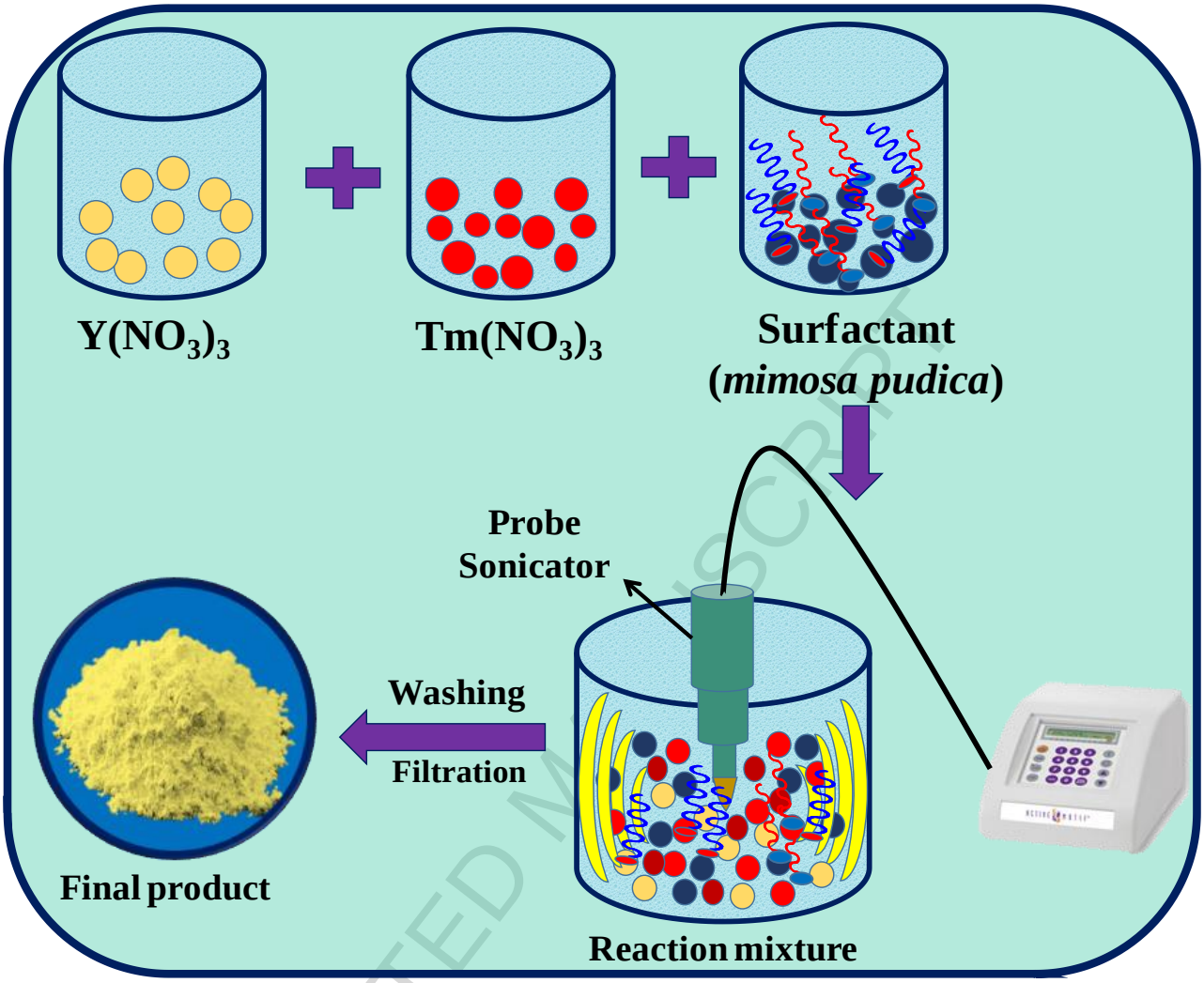

Fig.1. Schematic representation for the preparation of Y_2O_3: Tm^{3+} (1 -11 mol %) nanophosphor using *M.P.* extract as a surfactant.

ACCEPTED MANUSCRIPT

ACCEPTED MANUSCRIPT

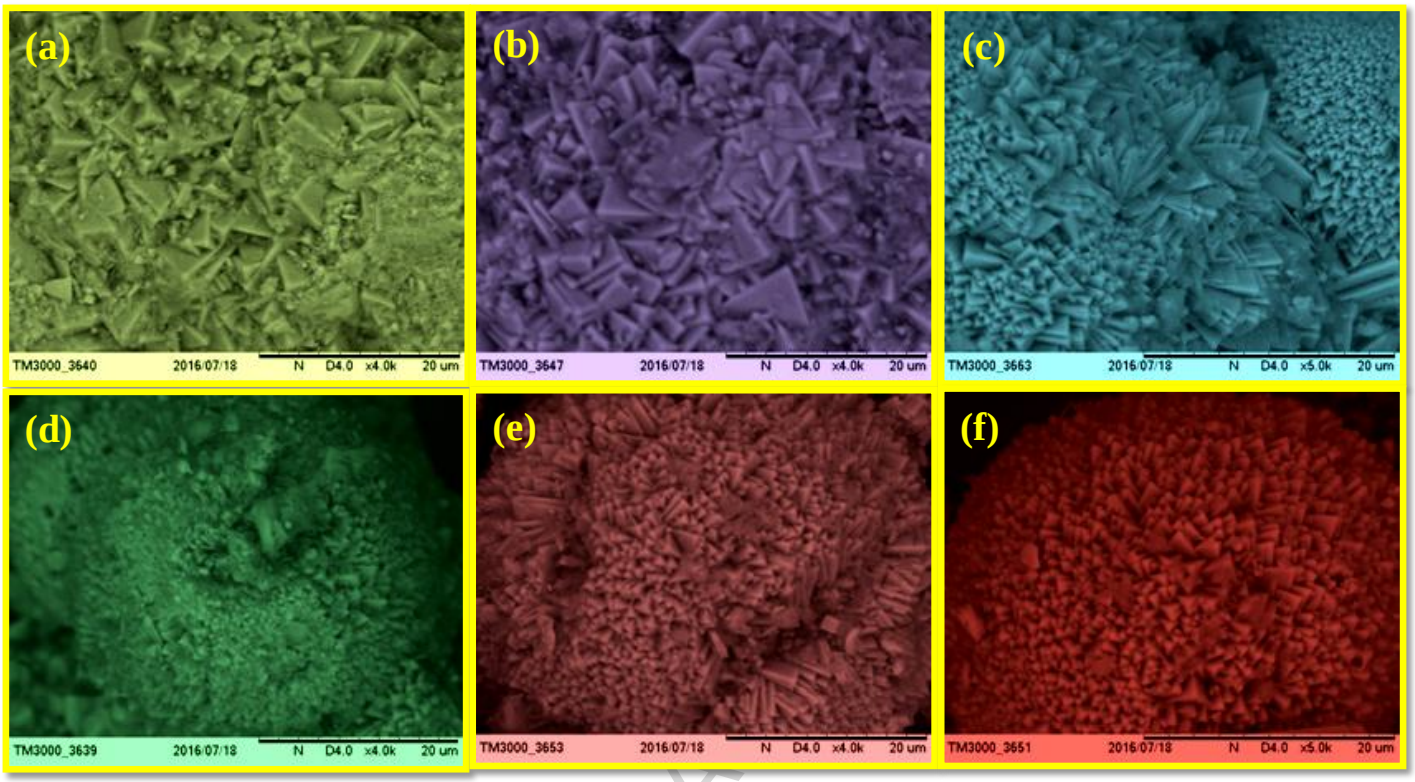

Fig. 2.SEM micrographs of Y_2O_3: Tm^{3+} (3 mol %) nanophosphor synthesized with different ultrasound irradiation time (1, 2, 3, 4, 5 and 6 h) while concentration *M.P.* surfactant and pH value of the solution were fixed at 30 % W/V and 9 respectively.

ACCEPTED MANUSCRIPT

ACCEPTED MANUSCRIPT

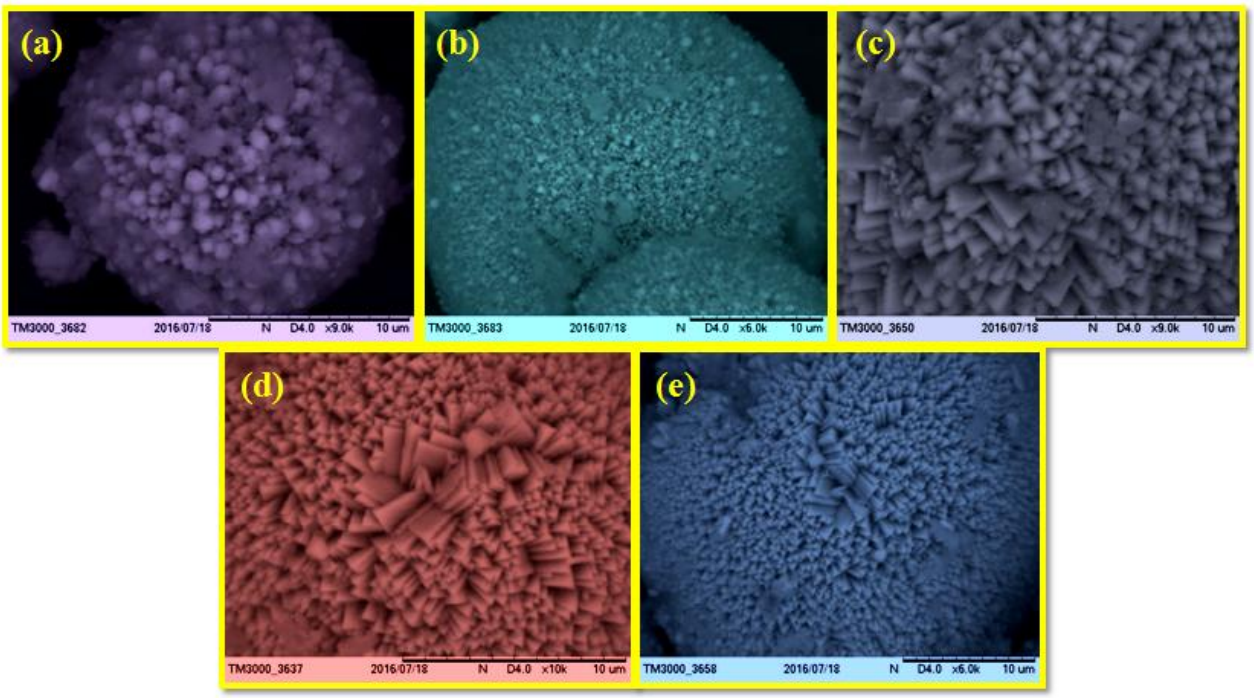

Fig.3. SEM micrographs of Y_2O_3: Tm^{3+} (3 mol %) nanophosphor synthesized with various concentration of *M.P.* surfactant (5, 10, 15, 20 and 30 % W/V) with 6 h of ultrasonic irradiation time and pH = 9.

ACCEPTED MANUSCRIPT

ACCEPTED MANUSCRIPT

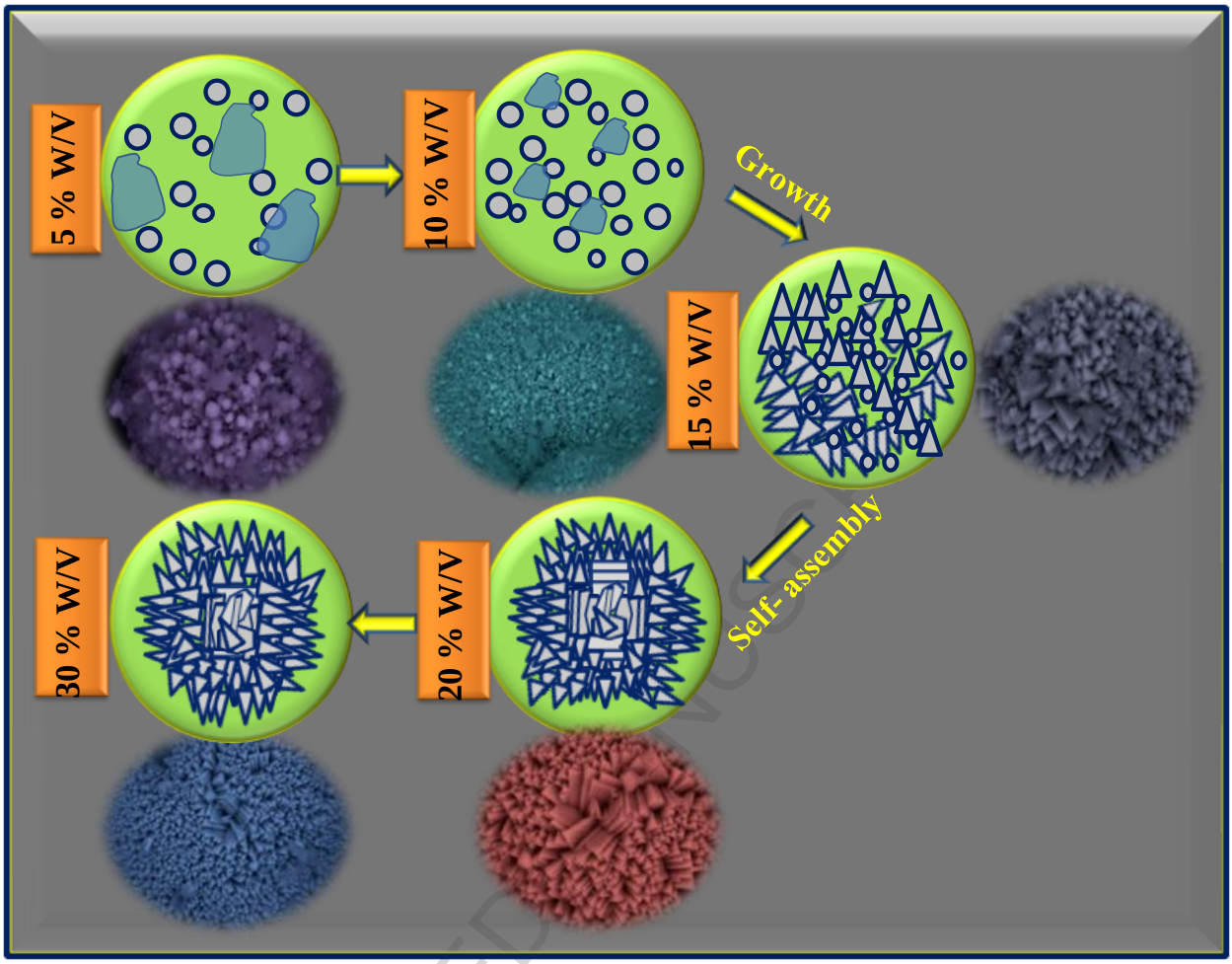

Fig.4. Schematic representation for the formation of Y_2O_3: Tm^{3+} nanophosphor with different concentration of *M.P*.

ACCEPTED MANUSCRIPT

ACCEPTED MANUSCRIPT

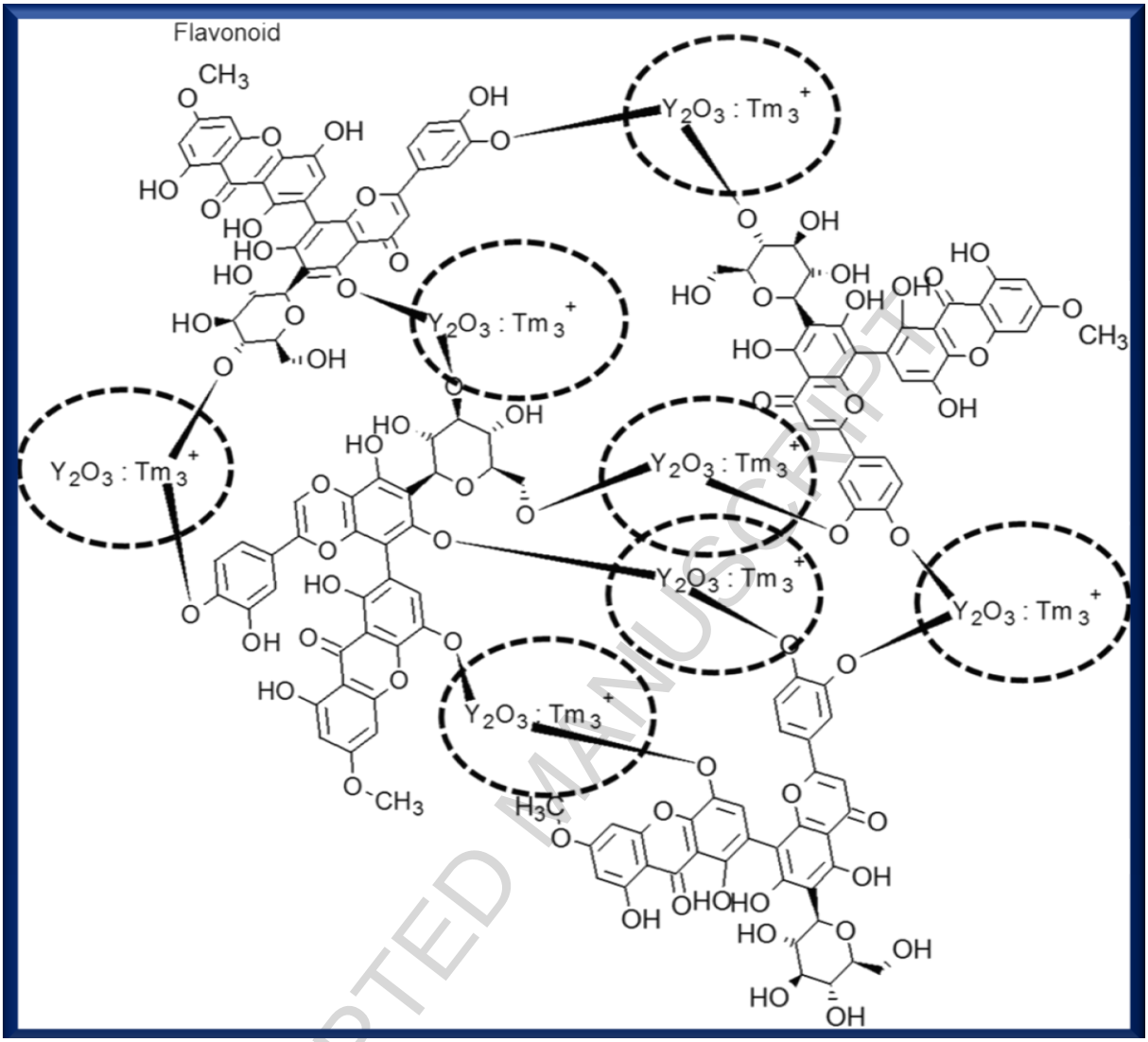

Fig.5. Possible egg box model for the trapping of Y_2O_3:Tm^{3+} ions in the network of flavonoids.

ACCEPTED MANUSCRIPT

ACCEPTED MANUSCRIPT

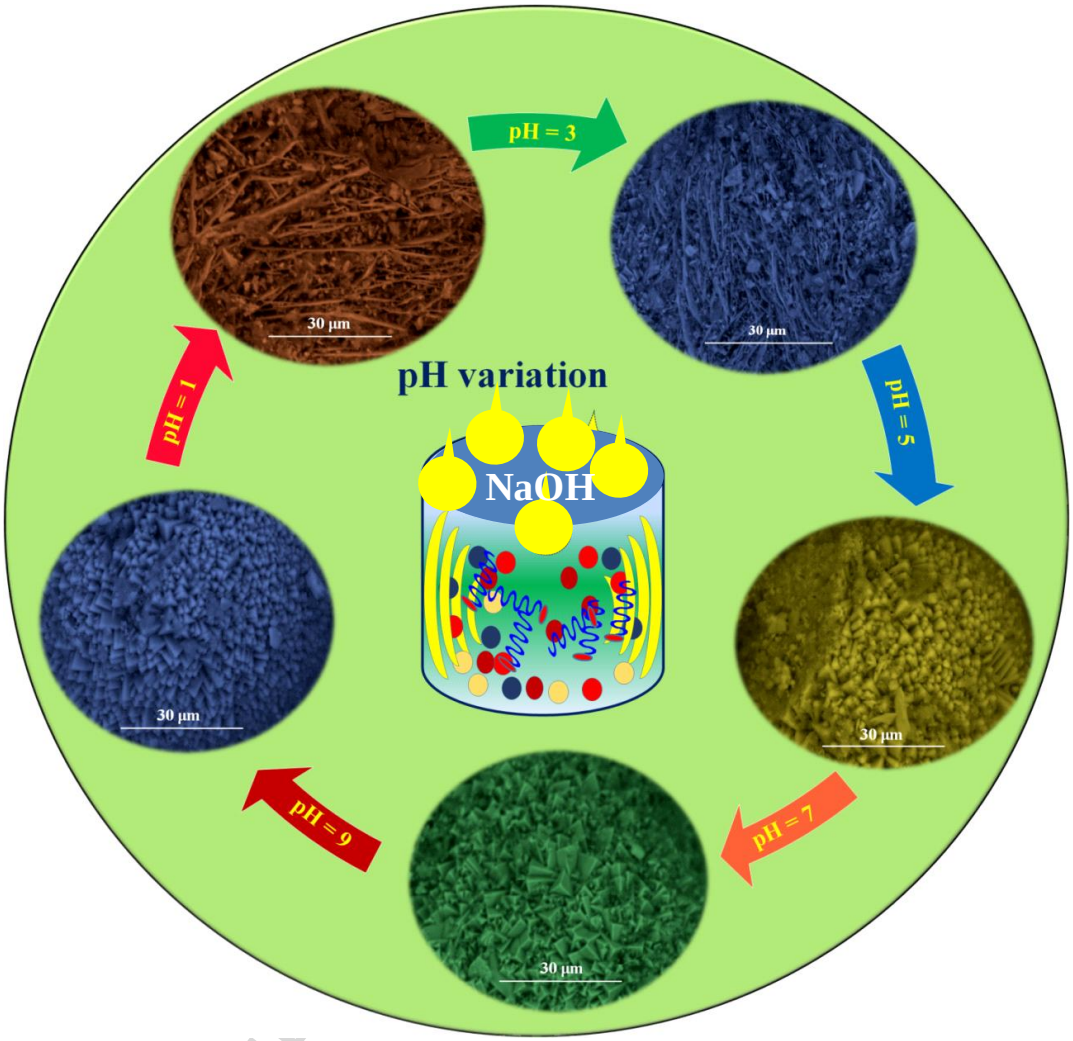

Fig.6. SEM images of Y_2O_3: Tm^{3+} (3 mol %) nanophosphor with various pH values (1, 3, 5, 7 & 9) in the presence of *M.P.* (30 % W/V) and 6 h irradiation time.

ACCEPTED MANUSCRIPT

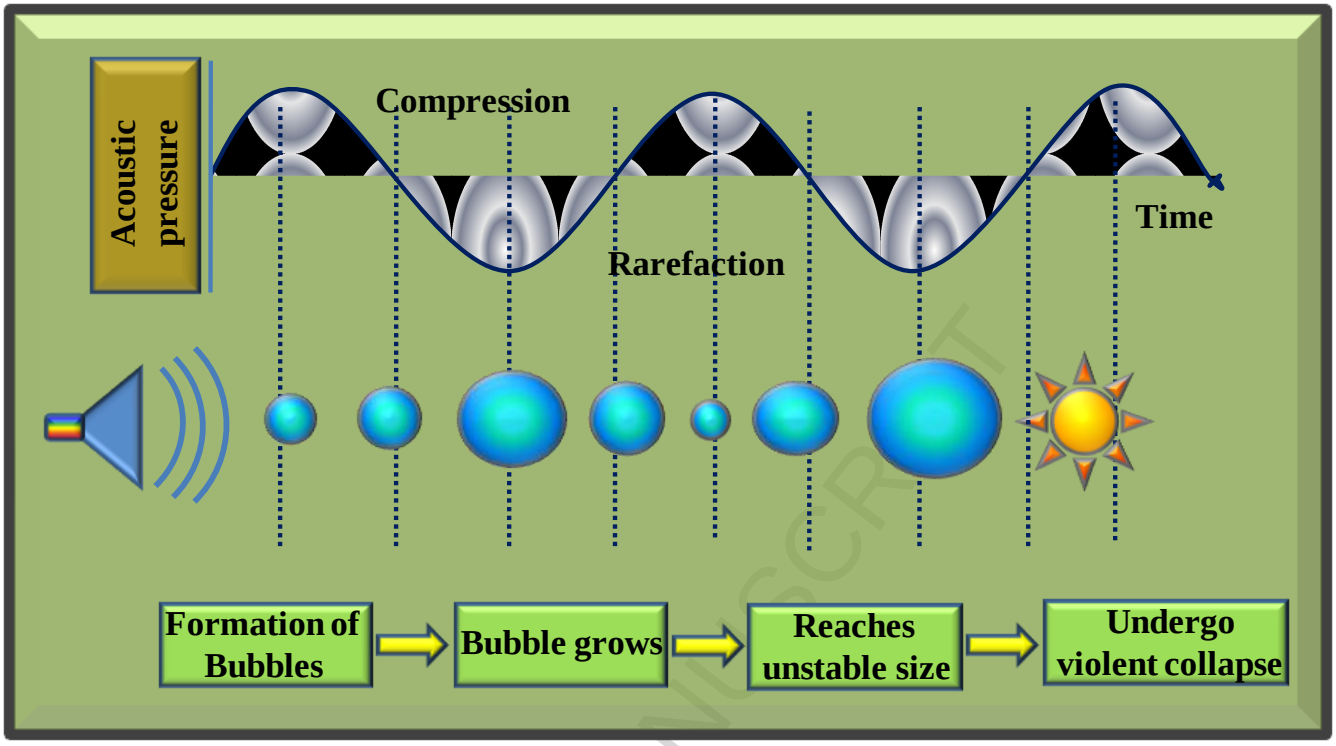

Fig.7. The schematic representation to demonstrate nucleation, growth and collapse of bubbles by ultrasound irradiation.

ACCEPTED MANUSCRIPT

ACCEPTED MANUSCRIPT

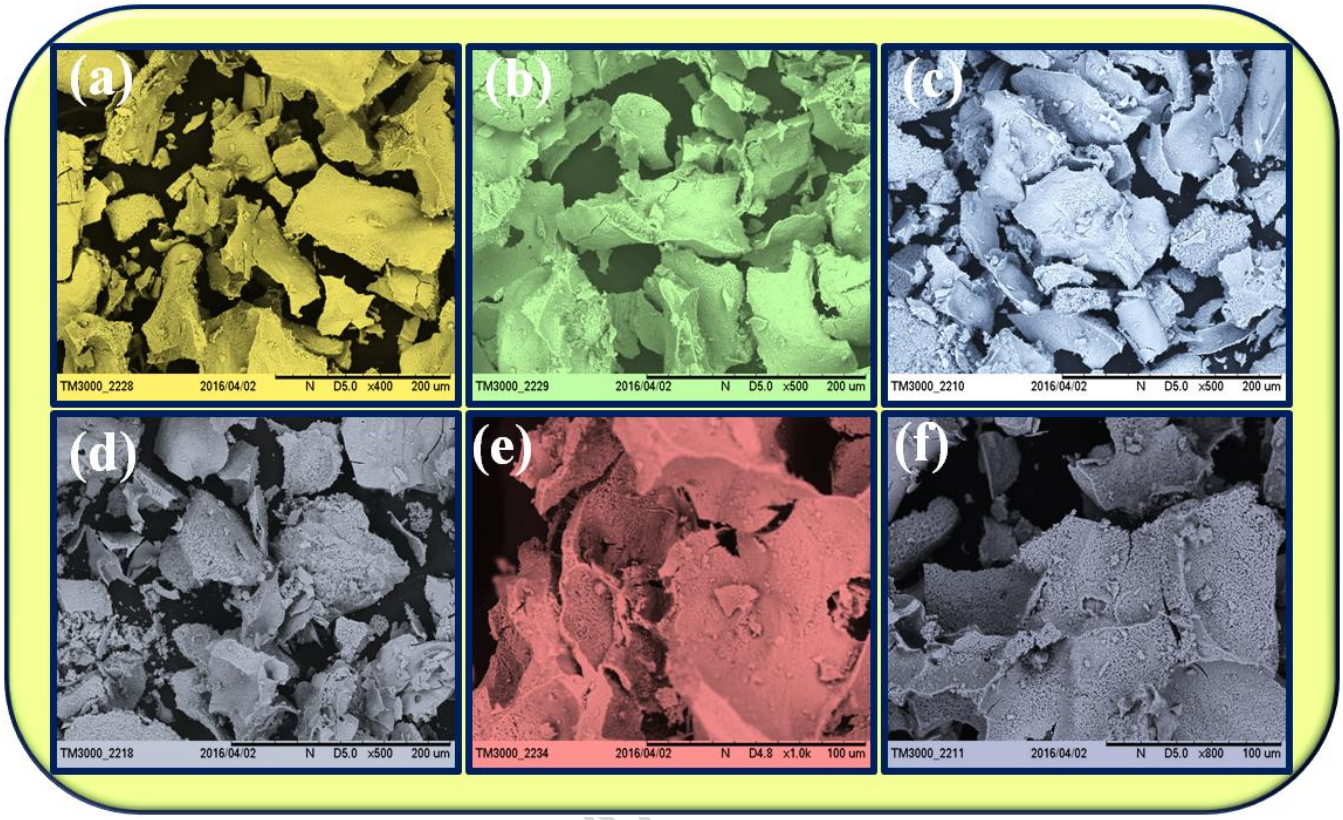

Fig.8. SEM micrographs of Y_2O_3: Tm^{3+} (3 mol %) nanophosphor under mechanical stirring in the absence of *M.P.* surfactant with different time (a) 1 h, (b) 2 h, (c) 3 h, (d) 4 h, (e) 5 h & (f) 6 h.

ACCEPTED MANUSCRIPT

ACCEPTED MANUSCRIPT

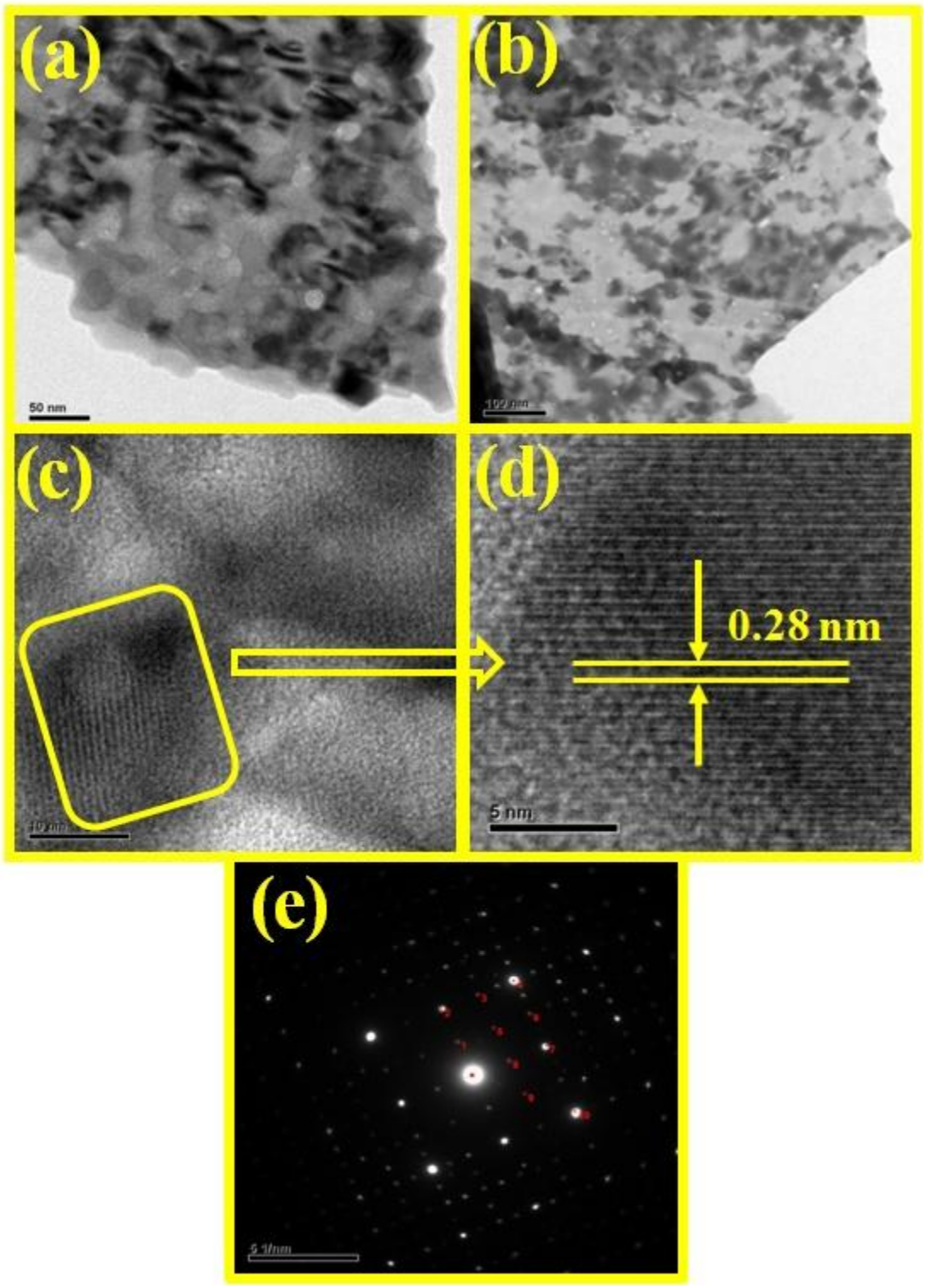

Fig.9. (a & b) TEM images, (c & d) HRTEM images and (e) SAED pattern of Y_2O_3: Tm^{3+} (3 mol %) nanophosphor.

ACCEPTED MANUSCRIPT

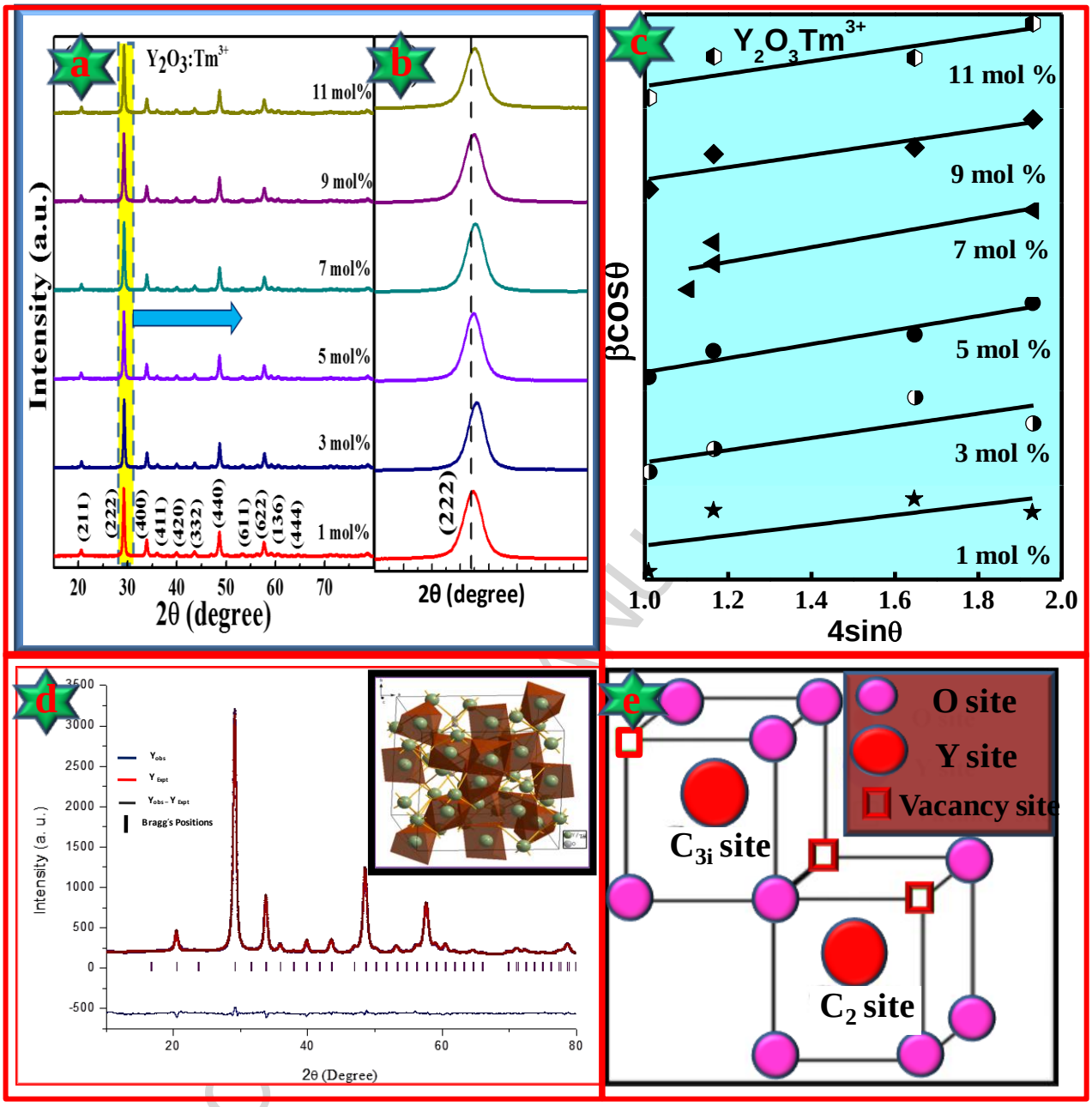

Fig.10. (a) PXRD patterns, (b) Shifting of (222) PXRD peak towards higher angle side, (c) W – H plots, (d) Rietveld refinement pattern (Inset: schematic representation of unit cell) and (e) cationic site symmetry of $Y_2O_3:Tm^{3+}$ (1 – 11 mol %) nanophosphor.

ACCEPTED MANUSCRIPT

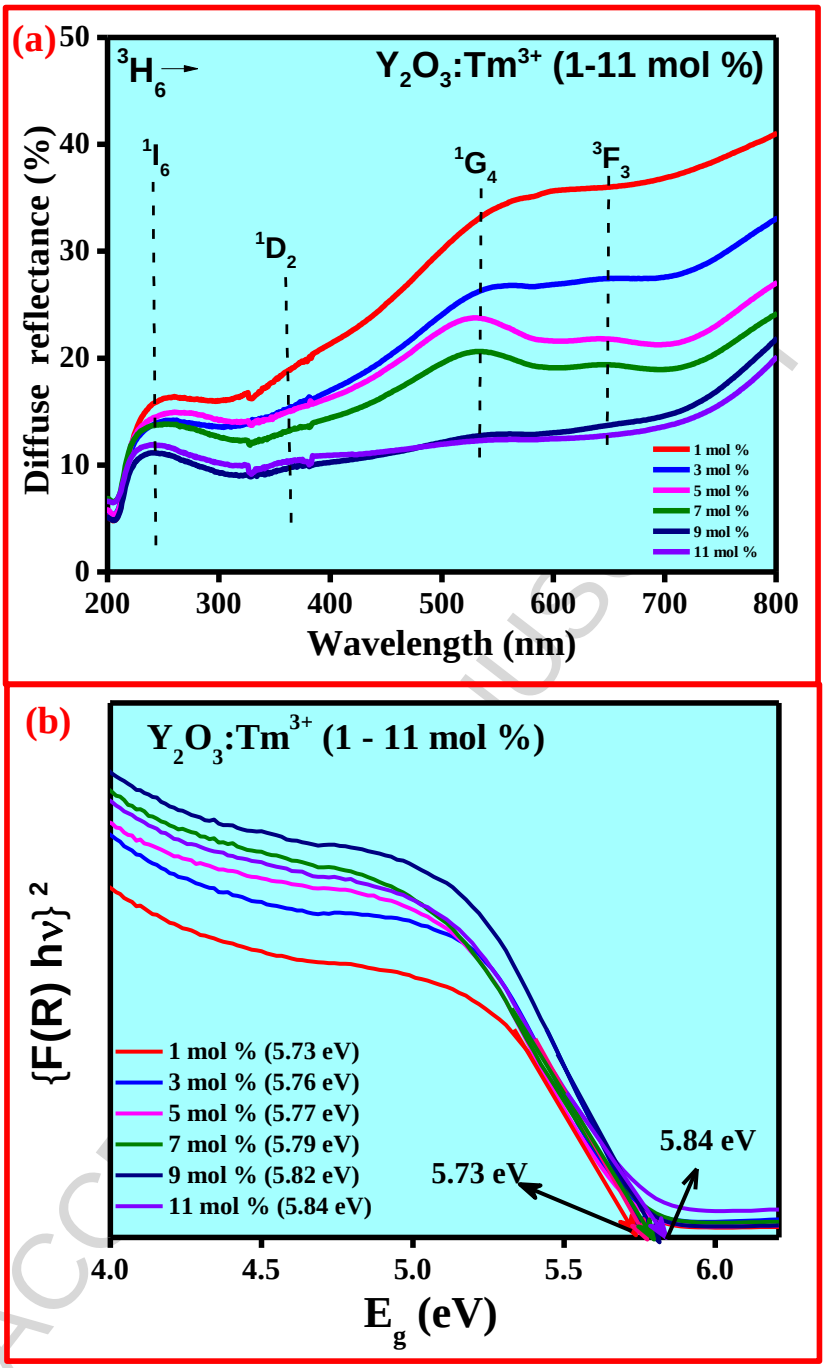

ACCEPTED MANUSCRIPT

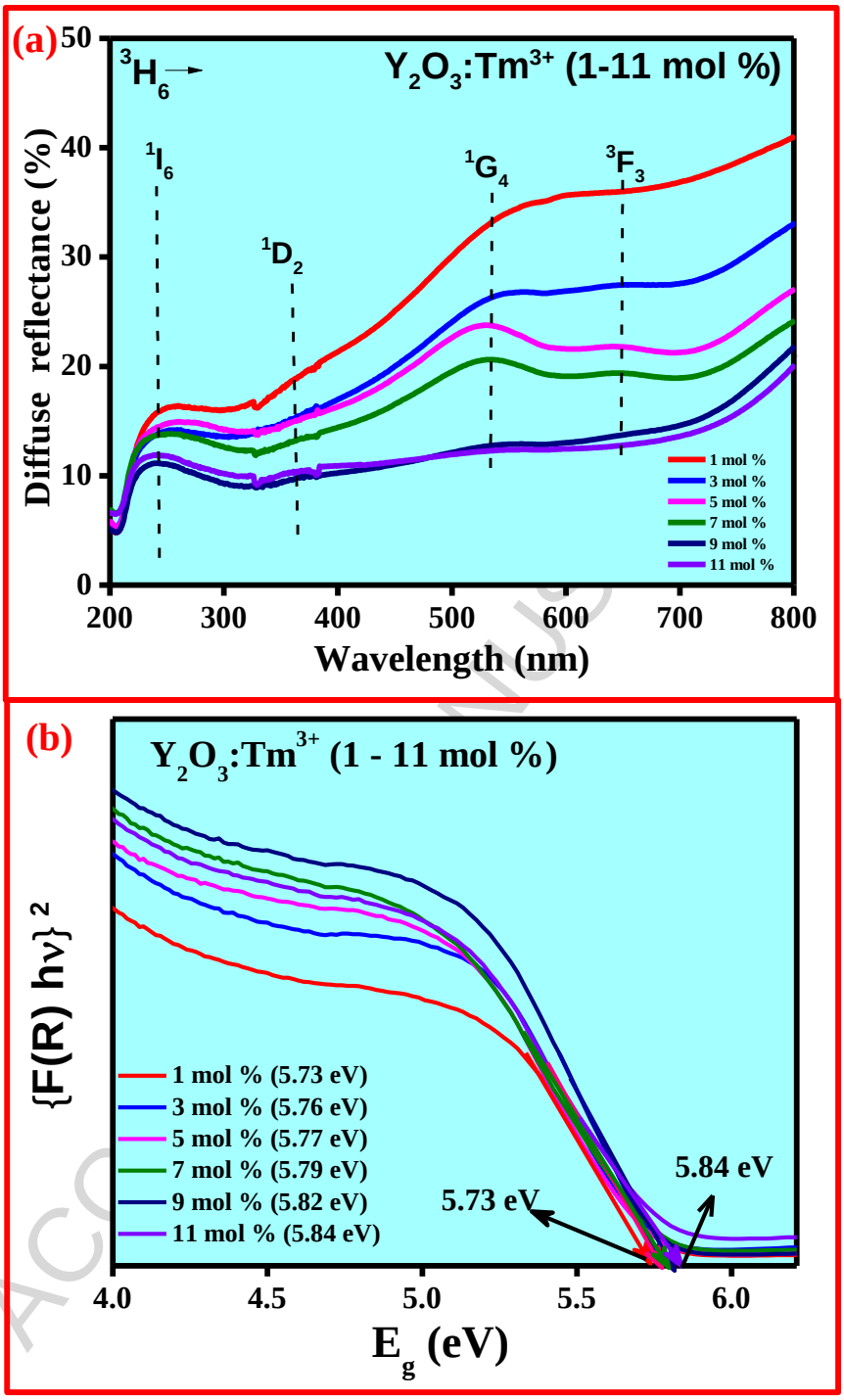

Fig.11. (a) DR spectra and (b) Energy band gap (E_g) of Y_2O_3:Tm^{3+} (1- 11 mol %) nanophosphor.

ACCEPTED MANUSCRIPT

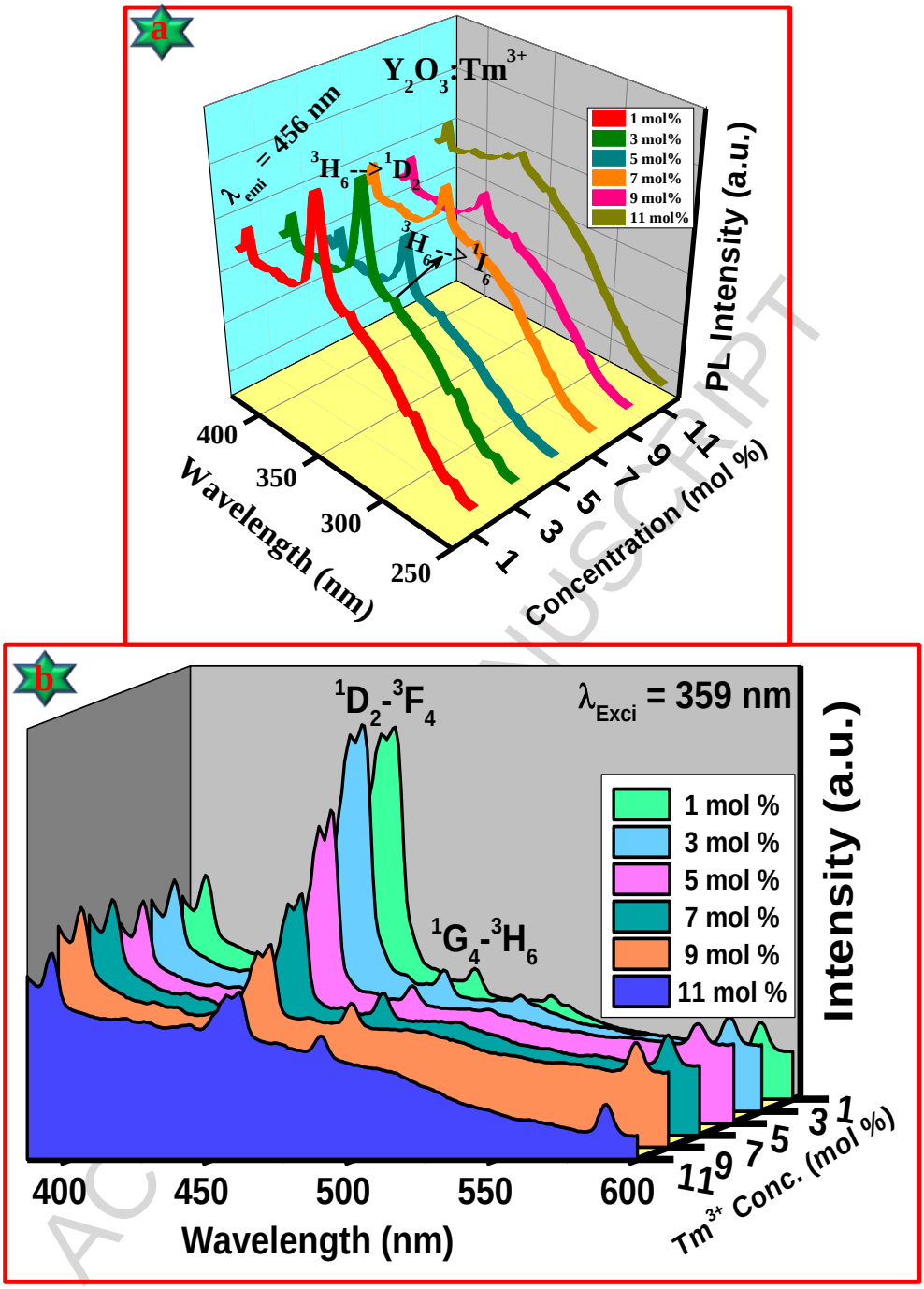

Fig.12 (a). PL excitation spectra and emission of $Y_2O_3:Tm^{3+}$ (1-11 mol %) nanophosphor.

ACCEPTED MANUSCRIPT

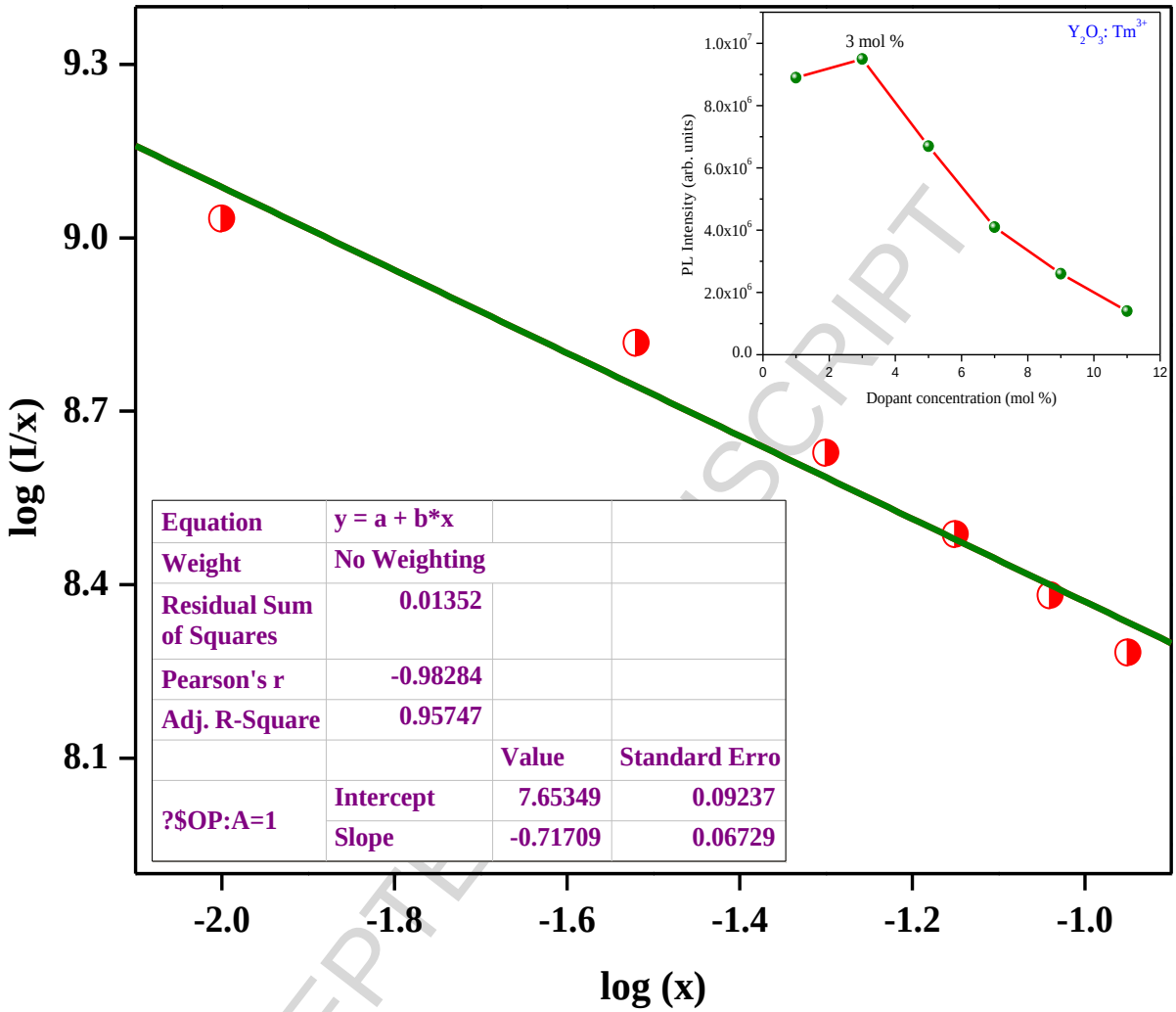

Fig.13. Logarithmic plot of (I/X) as a function of the concentration (X) (Inset: Variation of PL intensity with Tm^{3+} concentration).

ACCEPTED MANUSCRIPT

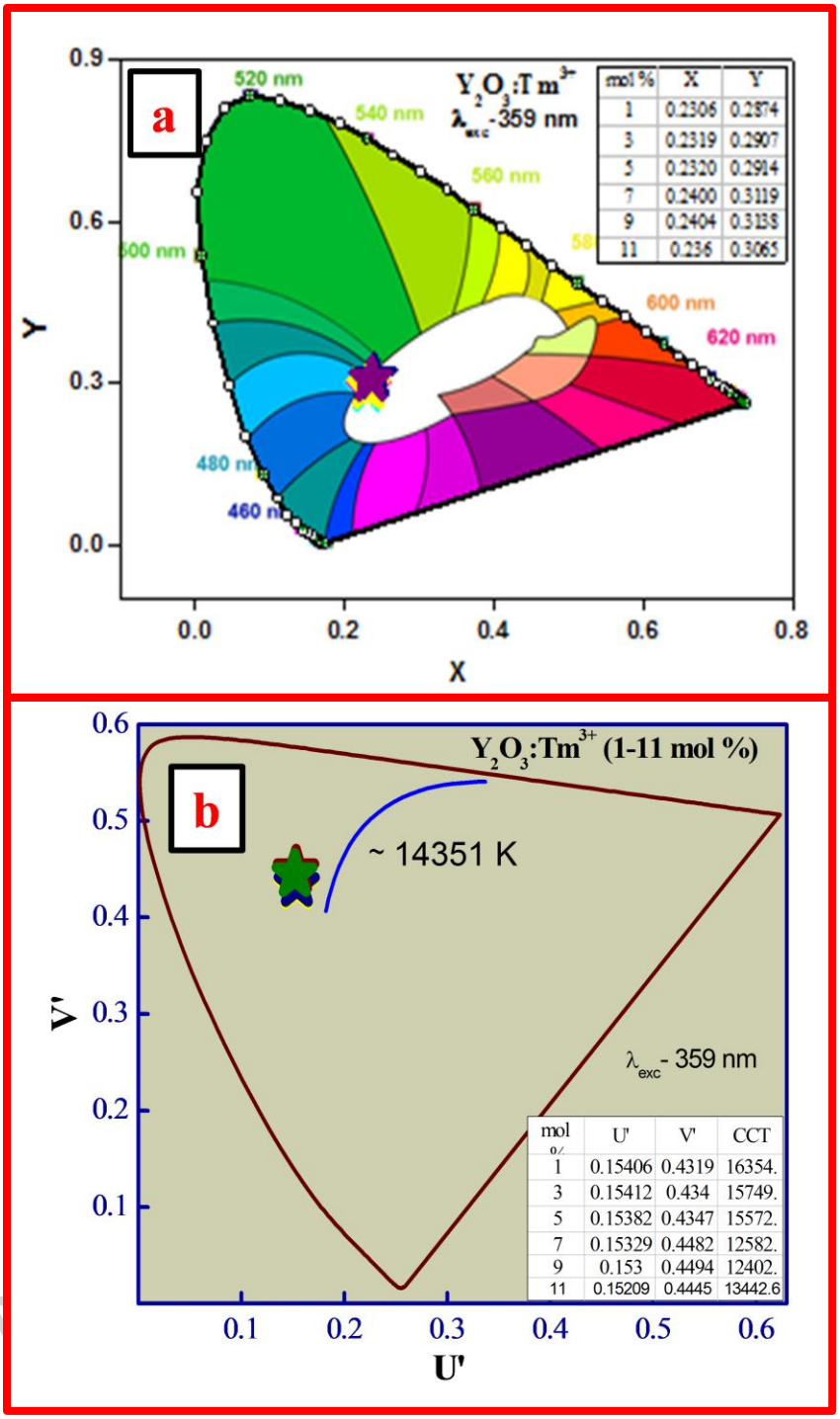

Fig.14(a). CIE chromaticity diagram and (b) CCT diagram of Y_2O_3: Tm^{3+} (1-11mol %) nanophosphor (Inset: Their corresponding CIE and CCT co-ordinates).

ACCEPTED MANUSCRIPT

Table.1. Estimated crystallite size, Full width half maxima (FWHM), strain and energy band gap (E_g) values of Y_2O_3: Tm^{3+} (1-11mol %) nanophosphor.

Y_2O_3: Tm^{3+} (mol %)	**FWHM (10^{-3} rad)**	**Crystallite size (nm)**		**Strain (ε) x 10^{-3}**	**E_g (eV)**
		Scherrer's method	**W-H method**		
1	6.99	21	19	1.2	5.73
3	8.25	17	17	1.8	5.76
5	7.87	18	15	0.68	5.77
7	8.30	17	21	1.6	5.79
9	8.96	16	19	1.2	5.82
11	8.84	16	21	1.45	5.84

ACCEPTED MANUSCRIPT

ACCEPTED MANUSCRIPT

Table.2. Rietveld refinement data of Y_2O_3: Tm^{3+} (1-11 mol %) nanophosphor.

Hermann-Mauguin Symbol with space group: I a -3 (206); Hall Symbol: -I 2b 2c 3; Crystal System: Cubic; Laue Class: m-3						
	Y_2O_3:Tm^{3+} (1 mol %)	**Y_2O_3:Tm^{3+} (3 mol %)**	**Y_2O_3:Tm^{3+} (5 mol %)**	**Y_2O_3:Tm^{3+} (7 mol %)**	**Y_2O_3:Tm^{3+} (9 mol %)**	**Y_2O_3:Tm^{3+} (11 mol %)**
a = b = c (Å)	10.6126 (2)	10.6068(5)	10.6041(1)	10.6040(3)	10.6142(2)	10.6049(3)
Cell Volume ($Å^3$)	1195.30	1193.30	1192.41	1192.37	1196.16	1192.324
X- ray Density (g/cm^3)	3.455	3.528	3.461	3.517	3.515	3.531
R_p	3.36	3.26	3.38	3.23	3.06	3.38
R_{wp}	6.37	7.17	7.29	7.13	6.88	7.27
R_{exp}	7.25	8.53	8.37	8.37	8.37	9.31
R_{Bragg}	2.93	1.87	2.15	1.80	1.60	1.77
R_F	4.04	2.43	2.80	1.81	1.64	1.96
χ^2	1.14	1.18	1.15	1.17	1.22	1.28
Atomic Coordinates						
Y1						
x	-0.0278	-0.0297	-0.02785	-0.0293	-0.0297	-0.0297
y	0.0000	0.0000	0.0000	0.0000	0.0000	0.0000
z	0.2500	0.2500	0.2500	0.2500	0.2500	0.2500
Occupancy	0.9007(12)	0.8996(7)	0.9007(6)	0.8996(14)	0.8996(8)	0.8996(4)
Tm1						
x	-0.0278	-0.0297	-0.02785	-0.0293	-0.0297	-0.0297
y	0.0000	0.0000	0.0000	0.0000	0.0000	0.0000

ACCEPTED MANUSCRIPT

z	0.2500	0.2500	0.2500	0.2500	0.2500	0.2500
Occupancy	0.6274(15)	0.6325(12)	0.62740(10)	0.6325(1)	0.6326(7)	0.63256(11)
Y2						
x	0.2500	0.2500	0.2500	0.2500	0.2500	0.2500
y	0.2500	0.2500	0.2500	0.2500	0.2500	0.2500
z	0.2500	0.2500	0.2500	0.2500	0.2500	0.2500
Occupancy	0.3230(4)	0.3230(6)	0.32304(7)	0.3230(12)	0.3230(3)	0.3231(27)
Tm2						
x	0.2500	0.2500	0.2500	0.2500	0.2500	0.2500
y	0.2500	0.2500	0.2500	0.2500	0.2500	0.2500
z	0.2500	0.2500	0.2500	0.2500	0.2500	0.2500
Occupancy	2.1355(1)	0.1081(5)	0.0057(6)	0.1081(11)	0.1081(7)	0.1081(11)
O						
x	1.3911	1.3928	1.3914	1.3931	1.3932	1.3929
y	2.3418	2.3439	2.3452	2.3456	2.3446	2.3439
z	0.8673	0.8792	0.8804	0.8818	0.8828	0.8792
Occupancy	2.3650(2)	2.1962(7)	2.1290(12)	2.1584 (17)	2.1828(18)	2.1962(13)

ACCEPTED MANUSCRIPT

ACCEPTED MANUSCRIPT

Table.3. Judd – Ofelt intensity parameters, radiative transition probability, radiative lifetime and branching ratio of Y_2O_3: Tm^{3+} (1-11 mol %) nanophosphor.

Tm^{3+} conc. (mol %)	**J–O intensity parameters ($\times 10^{-20}$ cm^2)**		**A_T (s^{-1})**	**τ_{rad} (ms)**	**β_R**
	Ω_2	**Ω_4**			
1	2.7	2.56	163	6.1	0.994
3	2.6	2.52	154	6.4	0.985
5	3.1	2.53	164	6.5	1.06
7	3.3	2.71	177	5.7	1.0
9	2.8	2.52	156	6.6	1.02
11	3.2	2.81	172	5.7	0.98

ACCEPTED MANUSCRIPT

ACCEPTED MANUSCRIPT

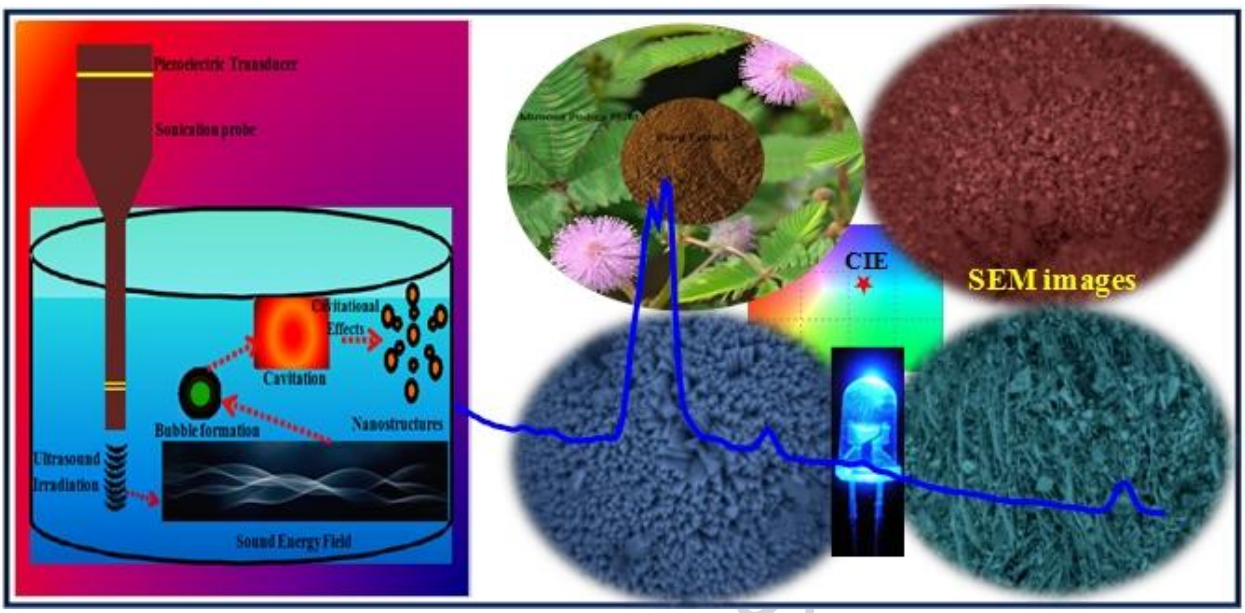

Graphical Abstract

ACCEPTED MANUSCRIPT

ACCEPTED MANUSCRIPT

Highlights:

- Y_2O_3:Tm^{3+} nanophosphors were prepared via modified sonochemical method.
- Prepared nanophosphors were characterized by techniques advanced techniques.
- Blue light emitting photoluminescence property was exhibited by the samples.
- Prepared samples were potential candidate for cool white light emitting display.

ACCEPTED MANUSCRIPT